Acta Crystallographica Section D
Biological Crystallography
ISSN 0907-4449

Structure of an RNA duplex r(GGCG$_{Br}$UGCGCU)$_2$ with terminal and internal tandem G·U base pairs

Ryuji Utsunomiya,[a,b,c] Kyoko Suto,[b] Dhakshnamoorthy Balasundaresan,[b] Akiyoshi Fukamizu,[a] Penmetcha K. R. Kumar[b] and Hiroshi Mizuno[a,b,c,d]*

[a]Institute of Applied Biochemistry, University of Tsukuba, Tsukuba, Ibaraki 305-8572, Japan, [b]Functional Nucleic Acids Group, Institute for Biological Resources and Functions, National Institute of Advanced Industrial Science and Technology (AIST), Central 6, Tsukuba, Ibaraki 305-8566, Japan, [c]Department of Biochemistry, National Institute of Agrobiological Sciences, Tsukuba, Ibaraki 305-8602, Japan, and [d]VTC Center, NEC Soft Ltd, Koto-ku, Tokyo 136-8627, Japan

Correspondence e-mail: mizuno-hiroshi@aist.go.jp

Received 30 September 2005
Accepted 25 December 2005

PDB Reference:
r(GGCG$_{Br}$UGCGCU)$_2$, 2ao5, r2ao5sf.

The crystal structure of a self-complementary RNA duplex r(GGCG$_{Br}$UGCGCU)$_2$ with terminal G·U and internal tandem G·U base pairs has been determined at 2.1 Å resolution. The crystals belong to the tetragonal space group $P4_3$, with unit-cell parameters $a = b = 37.69$, $c = 96.28$ Å and two duplexes in the asymmetric unit. The two strands of each duplex are related by a pseudodyad axis. The structure was refined to final R_{work} and R_{free} values of 20.9 and 25.3%, respectively. The duplexes stack in an end-to-end manner, forming infinite columns along the c axis. This is the first structural study of an RNA duplex containing G·U pairs at the termini. The stacking overlaps of the terminal G·U base pairs with their adjacent Watson–Crick base pairs are larger than those of Watson–Crick base pairs of the 5′-YR-3′/3′-RY-5′ type. The terminal G·U base pairs of neighbouring duplexes are also stacked with each other. An alternating underwound–overwound pattern of the twist angles is seen at each step along the duplex. This observation is typical for internal tandem G·U pairs, while the terminal G·U base pairs exhibit high twist angles with the adjacent Watson–Crick pairs. The 3′-side of U of the internal G·U base pair, which is unstacked, appears to be stabilized by π-cation interaction with an Mg^{2+} ion.

1. Introduction

The occurrence of the non-complementary G·U base pair was initially envisioned by Crick in his wobble hypothesis for the codon–anticodon interaction (Crick, 1966). G·U base pairs are the most common non-complementary base pairs and have been implicated in several biological functions: for example, G·U pairs are known to be responsible for the recognition of alanine tRNA by its cognate synthetase (Park *et al.*, 1989), for group I folding and ribozyme catalysis (Strobel & Cech, 1995, Adams *et al.*, 2004), to function in RNA editing (Simpson & Thiemann, 1995) and to participate in the regulation of ribosomal protein S15 expression (Benard *et al.*, 1998; Nikulin *et al.*, 2000). Moreover, G·U pairs are frequently observed in the stems of tRNA (He *et al.*, 1991; Wu *et al.*, 1995) and rRNA (Gutell *et al.*, 1994; Gautheret *et al.*, 1995; Szymanski *et al.*, 2000) secondary structures.

Some time ago, Mizuno and Sundaralingam proposed the occurrence of a G·U pair at the end of a helix to be governed by the following rule (Mizuno & Sundaralingam, 1978). The G·U base pair exhibits strikingly greater stacking overlap with the Watson–Crick base pair following it on the 3′-side of G (referred to as the 5′-end G·U pair) than with the Watson–Crick base pair preceding it on the 5′-side of G (referred to as the 3′-end G·U pair or as the 5′-end U·G pair). Indeed, G·U base pairs at the ends of helical stems of tRNAs are invariably

Table 1
Crystal data and refinement statistics.

Values in parentheses are for the highest resolution shell.

Duplex	r(GGCG$_{Br}$UGCGCU)$_2$
Wavelength (Å)	0.921
Space group	$P4_3$
Unit-cell parameters (Å)	$a = b = 37.69$, $c = 96.28$
Asymmetric unit	4 strands (2 duplexes)
Resolution range (Å)	30–2.1 (2.15–2.1)
No. of unique reflections	7838 (750)
Multiplicity	11.3 (11.6)
Completeness (%)	99.5 (99.6)
R_{merge} (%)	6.8 (20.3)
$I/\sigma(I)$	36 (19.1)
Final R/R_{free} (%)	20.9 (25.3)
No. of water molecules	251
No. of magnesium ions	1
R.m.s. deviation from ideality	
Bond length (Å)	0.004
Bond angle (°)	0.8

the '5′-end G·U pair' type (Mizuno & Sundaralingam, 1978). The preference for the '5′-end G·U pair' has also been observed in rRNA (Gautheret *et al.*, 1995). The geometry of Crick's wobble G·U base pair was first confirmed in the crystal structures of tRNA (Stout *et al.*, 1976; Westhof *et al.*, 1988), the 30S ribosomal subunit in complex with mRNA and tRNA^{Phe} (Ogle *et al.*, 2001) and in an RNA dodecamer at high resolution (Holbrook *et al.*, 1991). Since then, many other RNA oligomer structures containing G·U pairs have been reported. These G·U pairs are always internal G·U pairs. This is because the G·U base pair has irregular geometry, which is stabilized primarily by stacking interactions with the adjacent Watson–Crick base pairs, whereas a terminal G·U base pair can stack only with one side of a Watson–Crick base pair. However, nucleotides from the outgoing or ingoing loops or remote structural elements such as solvent molecules might interact on the other side and contribute to stabilize the terminal G·U base pair.

Monovalent and divalent cations, in particular Mg^{2+} ions, are well known to be essential for the folding and stability of large RNA molecules and to stabilize the tertiary structures. When a cation binds to the G·U base pair, the binding site is usually its major-groove side. On the other hand, networks of water molecules surrounding the RNA duplex (Egli *et al.*, 1976; Masquida & Westhof, 2000) and DNA duplex (Arai *et al.*, 2005) have been reported. Although the latter report includes no wobble base pairs, the analysis is based on a recent neutron diffraction study (Niimura *et al.*, 2005) in which water orientation is discussed in detail. Extensive hydration in both the major and minor grooves plays an important role in stabilizing the formation of the individual base pairs, including G·U base pairs, through linking between paired bases,

5′-GGC G $_{Br}$U G CGC U-3′
3′-UCG C G $_{Br}$U GCG G-5′

Figure 1
The self-complementary RNA duplex r(GGCG$_{Br}$UGCGCU)$_2$.

between base and ribose or between base and phosphate moieties.

To clarify the geometry surrounding the terminal G·U pairs, in this study we designed a self-complementary RNA duplex r(GGCG$_{Br}$UGCGCU)$_2$, which can form '5′-end G·U pairs' and internal tandem G·U pairs when arranged in a self-complementary manner (Fig. 1), and determined its crystal structure. In the crystal, the terminal G·U base pairs are stabilized by inter-duplex interactions through base overlaps of G and hydrogen bonds involving the phosphate and ribose O atoms of U. In addition, the present study provided detailed insights about the geometry, including the stacking interactions.

2. Materials and methods

2.1. RNA synthesis and purification

The decamer oligonucleotide r(GGCG$_{Br}$UGCGCU) was synthesized using standard solid-phase phosphoramidite chemistry on an automated nucleic acid synthesizer (Applied Biosystems DNA/RNA synthesizer, Model 394) using standard protocols with a 12 min coupling step. The oligonucleotide was cleaved from the solid support with 2 ml 3:1(*v*/*v*) ammonia/ethanol and was incubated overnight at 328 K for deprotection. After evaporation, the 2′-hydroxyl groups were deprotected by a 24 h incubation with 0.75 ml 1 *M* tetra-

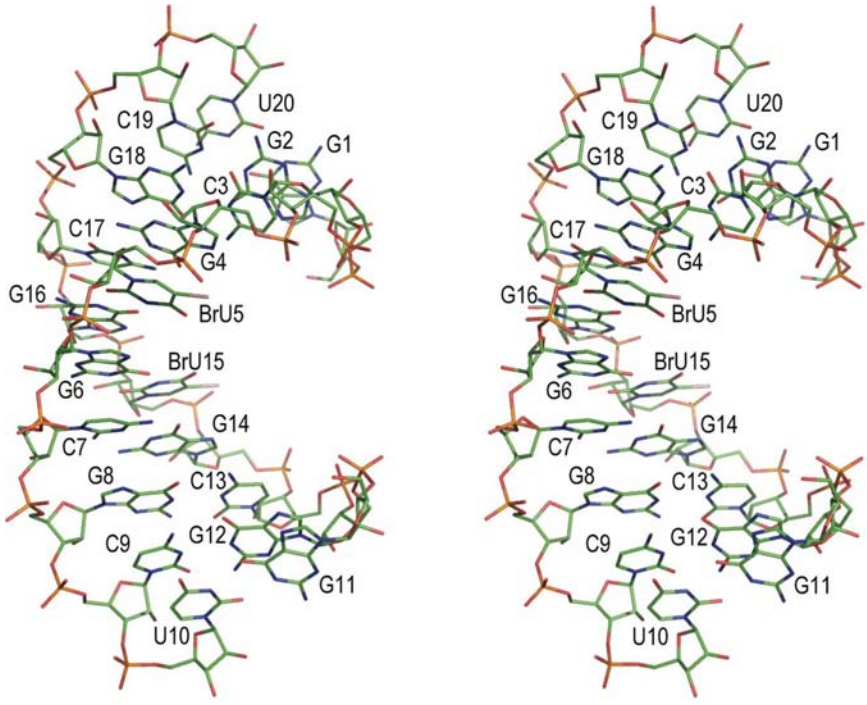

Figure 2
The overall structure of the decamer duplex (duplex *A*), shown in stereo.

butylammonium fluoride at room temperature using a dialysis membrane with a molecular-weight cutoff (MWCO) of 1000 Da (Spectra/Por; Spectrum Laboratories Inc.). An equal amount (0.75 ml) of 0.1 *M* triethylamine acetate was added and the mixture was dialyzed overnight against distilled water. The mixture was lyophilized and was further purified by 20% polyacrylamide gel electrophoresis. The relevant gel piece was excised and the oligonucleotide was eluted by electrophoresis. After filtration, the sample was lyophilized.

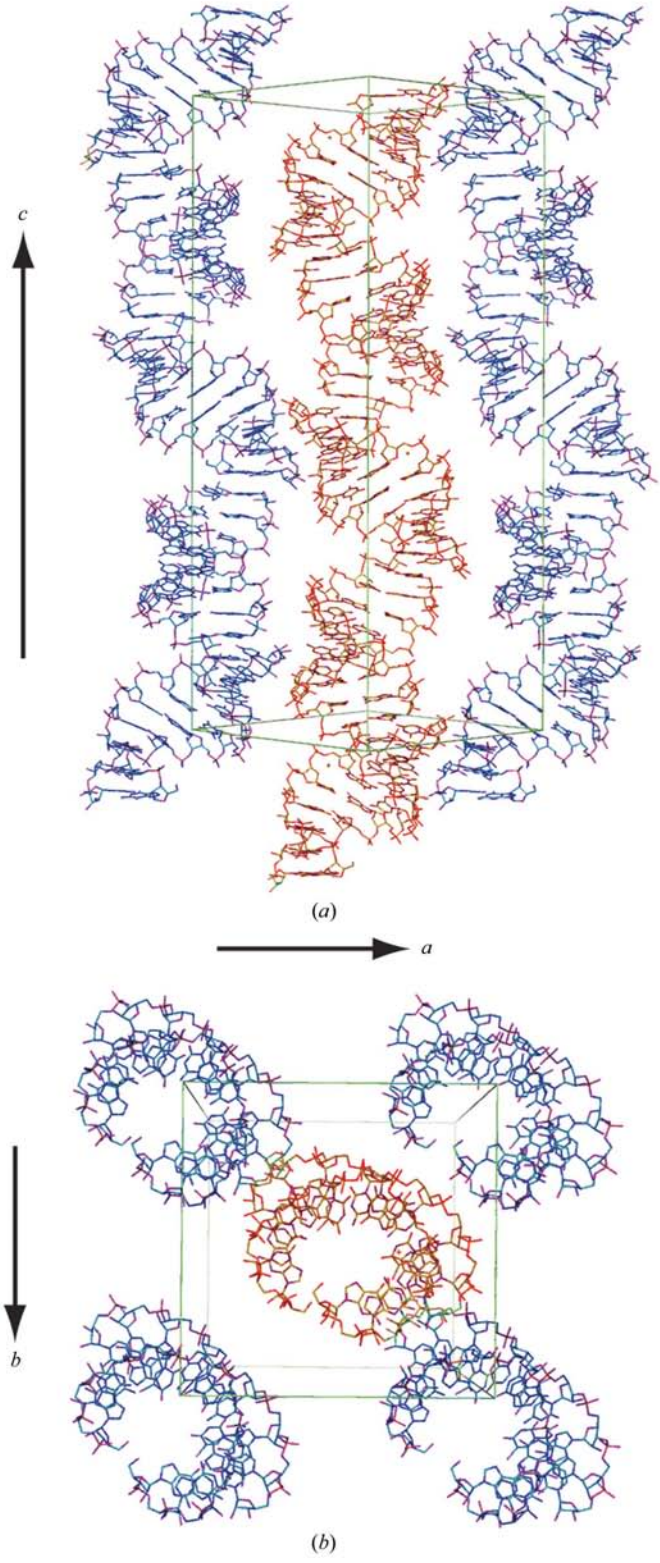

Figure 3
Crystal packing in the unit cell, viewed perpendicular to the *c* axis (*a*) and down the *c* axis (*b*). Duplexes *A* (red) and *B* (blue) form individual infinite columns in an end-to-end fashion along the *c* axis. Overlapping duplexes were removed for clarity.

2.2. Crystallization and data collection

Crystallization experiments were performed using the hanging-drop vapour-diffusion method at 293 K. The best crystals appeared using 1 m*M* RNA, 25 m*M* MES buffer pH 6.0, 5 m*M* magnesium chloride and 0.5 m*M* spermine tetrachloride equilibrated against dissolution buffer supplemented with 30% 2-methyl-2,4-pentanediol (MPD). Crystals appeared within 2 d and grew to maximum dimensions of 0.3 × 0.3 × 0.8 mm. Diffraction studies were performed under cryo-conditions at Photon Factory BL-6B. Data were integrated and merged with the *HKL*2000 program suite (Otwinowski & Minor, 1997). The crystals belong to the tetragonal space group $P4_3$, with unit-cell parameters $a = b = 37.69$, $c = 96.28$ Å, and the asymmetric unit contains four RNA strands. Data-collection statistics are summarized in Table 1.

2.3. Structure solution and refinement

The Br-derivative of the RNA decamer was initially designed and prepared for anomalous scattering phasing, but before the anomalous method was performed the structure was solved by molecular replacement using *CNS* (Brünger *et al.*, 1998). A search model was derived by modifying the structure of an RNA duplex (PDB code 157d; Leonard *et al.*, 1994). *CNS* (Brünger *et al.*, 1998) was used for refinement. For cross-validation, a test data set was selected comprising 5% of the reflections. $R_{\rm free}$ was 45.4% at 2.5 Å resolution after a few cycles of rigid-body refinement. Two RNA duplexes, *A* and *B*, were unambiguously identified in the $2F_{\rm o} - F_{\rm c}$ electron-density maps. The model was gradually improved by alternating cycles of *CNS* refinement and model building using the *XtalView* program (McRee, 1999). Water molecules were then added to the model using alternating steps of the 'water pick' and 'water delete' procedures as implemented in the *CNS* program. The $F_{\rm o} - F_{\rm c}$ difference electron-density maps indicated an unidentified peak (of 7.9σ) near the phosphate O atom of G6 in the entrance of the major groove of duplex *A*. This peak was assigned as an Mg^{2+} ion considering the peak height and shape and the crystallization condition. The Mg^{2+} ion and four inner-sphere water molecules were then added to the model. Repeated cycles of positional refinement resulted in a significant drop in the *R* factor. The statistics of the final refinement are summarized in Table 1. Helical parameters and stacking overlaps were calculated using the 3*DNA* program (Olson *et al.*, 2001).

3. Results and discussion

3.1. Overall structure

The asymmetric unit consists of two duplexes. The two independent strands in each duplex are related by a pseudo-twofold axis. The two duplexes, *A* and *B*, are very similar to each other, with an r.m.s.d. of 0.74 Å, and so hereafter we only refer to duplex *A* unless otherwise noted. The structure of duplex *A* is shown in Fig. 2. Duplex *A* stacks in an end-to-end fashion, forming a pseudo-continuous column, and duplex *B* forms another pseudo-continuous column in a similar manner. The stacked duplexes are closely packed around the 4_3 screw axis parallel to the crystallographic *c* axis (Fig. 3). At the junction, the helices stack onto each other with a negative helical twist of −40° (Fig. 4*a*), forming a pseudo-infinite helix with an underwound step at the junction. All the ribose sugars are in the characteristic C3′-*endo* conformation. The intra-chain phosphate–phosphate distance is in the range 5.5–6.2 Å, which is typical for chains containing a C3′-*endo* sugar pucker, except for distances of 6.8 Å for G6–C7 and G14–BrU15 in duplex *A* and 6.7 Å for G4–BrU5, 6.6 Å for G6–C7 and 6.5 Å for G14–BrU15 in duplex *B*, which all involve phosphates of the internal G·U pairs or the neighboring nucleotides. The dinucleotide steps are right-handed and in the usual range for A-form RNA, except for the BrU5–G6/BrU15–G16 steps in both duplexes. A torsional change occurs at the BrU5–G6 and C13–G14 steps in duplex *A*, where the α/γ angles of G6 and G14 move to a *gauche*$^+$/*trans* conformation, in contrast to the most frequently observed *gauche*$^-$/*gauche*$^+$ conformation. At C3–G4, BrU5–G6 and C13–G14 in duplex *B*, G4, G6 and G14 move to the *gauche*$^+$/*trans* conformation. These extended conformations are apparently correlated with the aforementioned phosphate–phosphate distances.

The RNA–RNA packing contacts are displayed in Fig. 4. The N2 atom and the 2′-hydroxyl group of G16(*A*) hydrogen bond with the 2′-hydroxyl group and the phosphate O atom O1P of U10(*B*) of the terminal G·U base pair, respectively (Fig. 4*b*). In another contact region (Fig. 4*c*), the two duplexes are held together by eight hydrogen bonds around a pseudo-twofold axis. In the top half of Fig. 4(*c*), the 2′- and 3′-hydroxyl groups of the terminal U10(*A*) hydrogen bond with the 2′-hydroxyl group of C3(*B*), the phosphate O atom of U10(A) hydrogen bonds with the 2′-hydroxyl group of G4(*B*) and the 2′-hydroxyl group of C9(*A*) hydrogen bonds with the N2 atom of G18(*B*). Analogous hydrogen bonds are observed in the pseudosymmetry-related region between G8(*A*), C13(*A*), G14(*A*) and C19(*B*) and U20(*B*) (bottom half of Fig. 4*c*).

3.2. Tandem G·U base pairs

The sequence (5′-UG-3′/3′-GU-5′) of the present tandem G·U base pairs is known as motif I and occurs most frequently in 16S and 23S rRNAs (Gautheret *et al.*, 1995). The present tandem G·U base pairs are sandwiched by the flanking Watson–Crick G·C base pairs, generating three types of stacking interactions (Figs. 5*b*, 5*c* and 5*d*). In the stacking pattern of the adjacent G·U pairs, the six-membered ring of G6 lies directly over the six-membered ring of G16 from the opposite strand, while BrU5 and BrU15 of the G·U base pairs lack stacking interactions within the G·U base pairs. The base

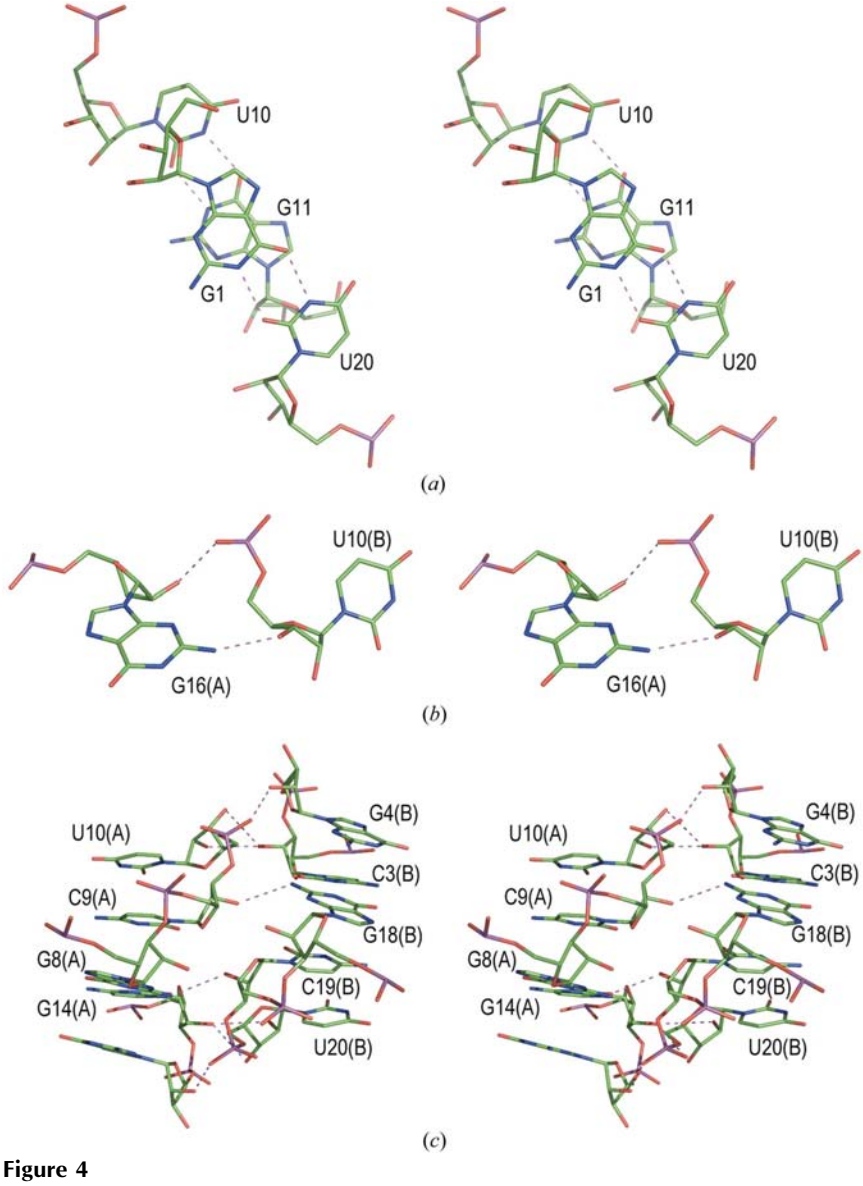

Figure 4
Inter-duplex interactions. Base stacking of the terminal G·U base pairs (*a*) and hydrogen bonds between duplexes *A* and *B* in the horizontal direction (*b* and *c*) are shown in stereo.

overlaps of these pyrimidine rings are compensated by stacking with their flanking Watson–Crick G·C base pairs on their 5′-sides. The six-membered ring of BrU5 stacks with the six-membered ring of G4 in the same strand (Fig. 5*b*) and similarly the six-membered ring of BrU15 stacks with the six-membered ring of G14 in the same strand (Fig. 5*d*). The Br atoms of BrU5 and BrU15 also contribute to a partial stacking. These distinct stacking patterns resemble those in the crystal structure of r(GUAUGUA)dC (Biswas *et al.*, 1997), which contains motif I tandem G·U pairs, although the flanking Watson–Crick base pairs are not G·C but A·U pairs. Based on the available crystal structures for motif I (5′-UG-3′/3′-GU-5′), motif II (5′-GU-3′/3′-UG-5′) and motif III (5′-UU-3′/3′-GG-5′), Deng & Sundaralingam (2000) ranked the stacking stabilities in the order motif I > motif III > motif II, which is consistent with their thermodynamic stabilities (He *et al.*, 1991; Wu *et al.*, 1995). Recent studies using molecular-dynamics simulations and quantum-mechanical calculations revealed a preference for 5′-UG-3′/3′-GU-5′ over 5′-GU-3′/3′-UG-5′ in a series of RNA octamers (Pan *et al.*, 2005). The present tandem G·U pairs and the flanking Watson–Crick base pairs may stabilize the central part of the duplex. Solvent molecules also contribute to the stability of duplex formation. Water molecules around G·U base pairs are located in the major and minor grooves. Fig. 5 shows the water molecules which hydrogen bond to the bases. Each G·U base pair has potential hydrogen-bonding sites: the O4 of U and the O6 and the N7 of G in the major groove and the O2 of U and the N2 and N3 of G in the minor groove. The most common hydration site of G·U pairs, located between the N2 of G and the O2 and O2′ of U in the minor groove (Masquida & Westhof, 2000; Trikha *et al.*, 1999), is conserved in the present tandem G·U pairs, but not in the terminal G·U pairs. However, the N3 has no specific hydration, as previously mentioned (Masquida & Westhof, 2000). In the inter-base pairs, one or two water-mediated hydrogen bonds between adjacent base pairs contribute to stabilization of the G·U base pair.

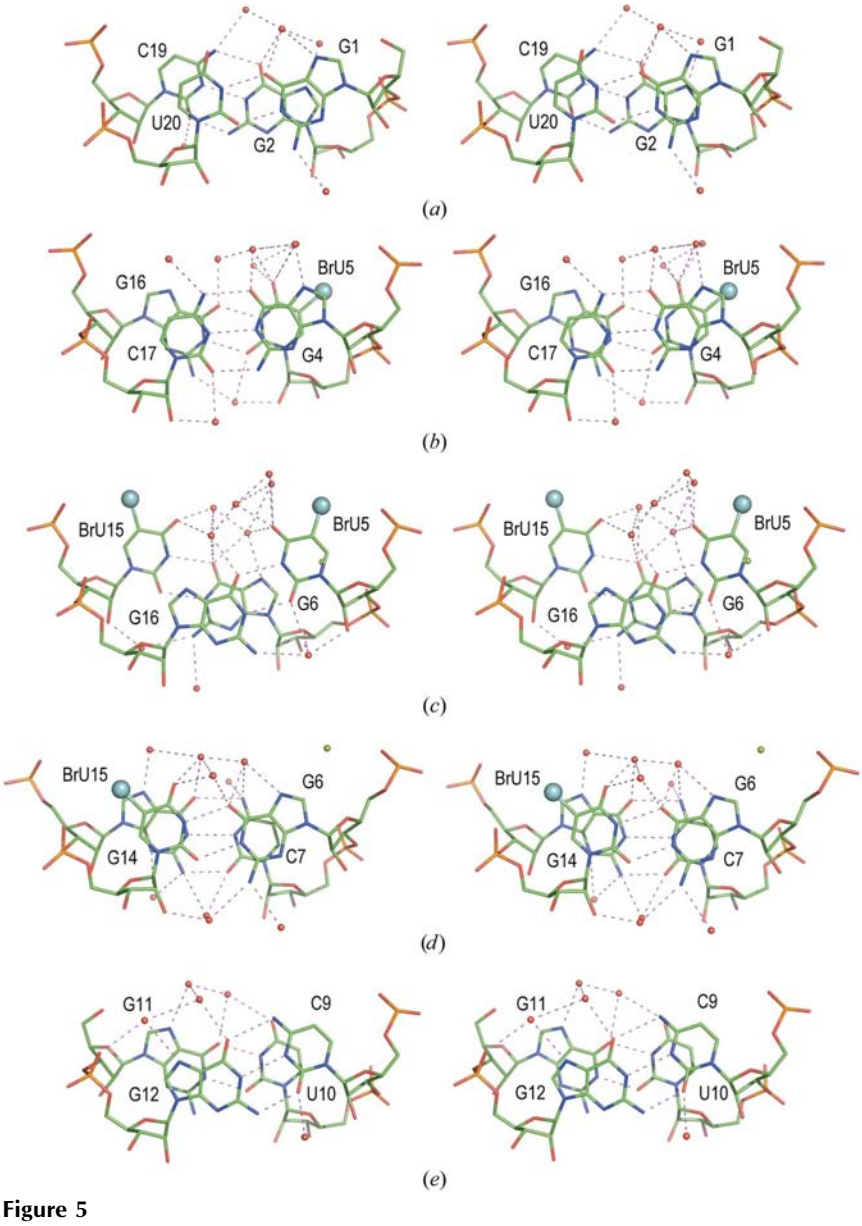

Figure 5
Stereo pairs of base stackings in terminal (*a* and *e*) and tandem base pairs (*b*, *c* and *d*) in duplex *A*. Large blue and small green spheres indicate Br atoms and Mg^{2+} ions, respectively. Red spheres indicate water molecules which hydrogen bond to bases.

3.3. Terminal G·U base pairs

The hydrogen-bonding pattern of the terminal G·U base pairs is the same as that of the tandem G·U base pairs. Fig. 5(*a*) shows the stacking interactions with the adjacent Watson–Crick G·C base pairs. The six-membered ring of G1 lies over the five-membered ring of G2, whereas the six-membered ring of U20 partially covers the six-membered ring of C19. The G·U base pair at the other end shows a similar stacking pattern (Fig. 5*e*). This stacking overlap is smaller than that of 5′-RY-3′ with the preceding base pair, but is slightly larger than that of 5′-YR-3′ with the preceding base pair (Fig. 6). The zigzag pattern of the base-stacking overlap in Fig. 6 apparently arises from the alternating purine–pyrimidine sequence of the decamer, except for the terminal bases. This base overlap is closely correlated with the twist angles at the step, as seen in Fig. 6. The twist angles between the tandem G·U pairs and their flanking pairs are typical. This underwound–overwound pattern of the twist angles of the G·U base-pair steps has previously been described in X-ray structures (Biswas & Sundaralingam, 1997; Masquida *et al.*, 1999; Masquida & Westhof, 2000; Trikha *et al.*, 1999). The terminal G·U base pairs in this

crystal are stabilized by inter-duplex interactions through the base stacking of G (Fig. 4*a*) and the hydrogen bonds involving the phosphate and ribose O atoms of U (Fig. 4*b*). In Fig. 4(*a*), the six-membered ring of G1 lies over the six-membered ring of G11 of the neighboring duplex. This base overlap is somewhat similar to that of the cross-strand stacking observed in the internal G·U base pairs (Fig. 5*c*), but the variation in the stacking manner arises from the difference in the twist angle.

3.4. Mg^{2+} binding

Mg^{2+} ions are well known to be essential for the folding and stability of large complex RNA structures such as those found in the ribosome and self-splicing introns, where Mg^{2+} ions stabilize tertiary structure by mediating interactions between their structural domains. However, in the case of small RNA or DNA duplexes, specific binding sites for Mg^{2+} ions are quite limited, although Mg^{2+} ions are required to neutralize the negative charges of phosphate groups. Consequently, Mg^{2+} ions would interact in a 'diffuse binding mode' involving nonspecific long-range electrostatic interactions with Mg^{2+} ions (Misra & Draper, 1998), which would not yield distinct electron-density peaks. Mg^{2+} ion interactions with small RNA oligomers can also be explained by the binding of a cloud of delocalized ions, as supported by Brownian dynamics simulations (Serra *et al.*, 2002). To date, only a few Mg^{2+}-bound oligonucleotide structures have been reported (Ennifar *et al.*, 2003; McFail-Isom *et al.*, 1998; Robinson *et al.*, 2000), in which Mg^{2+} ions usually bind to the N7 of Gs and to the phosphate groups and rest in the major groove, where they interact with the water shell as inner-sphere ligands. In the present structure, an Mg^{2+} ion is found at the 3′-side of BrU5 of the internal G·U base pair in duplex *A*. This unstacked base might serve as a platform for trapping Mg^{2+} ions through the π-system of the bases. Only BrU5 and BrU15 have unstacked bases in the base-pair steps (Fig. 5); the extended conformation of the backbone of G6 can provide a wider space for Mg^{2+}-binding at the 3′-side of BrU5 than that of BrU15. Mg^{2+} ion-binding is thus localized mainly by interaction with the face of the π-system of BrU5. The distance from the Mg^{2+} ion to the ring centroid is 3.65 Å, suggesting a cation–π interaction. The existence of a cation–π interaction is also consistent with earlier results, where the π-system involved either inner-sphere or outer-sphere coordination (Zaric *et al.*, 2000; McFail-Isom *et al.*, 1998). Within the P4–P6 domain of tetrahymena group I ribozyme, four Mg^{2+} ions are located less than 5 Å from the centroids of the adenine imidazole ring (McFail-Isom *et al.*, 1998). A common motif is that in which the Mg^{2+} ion interacts with both a lone pair of the phosphate and the π-electrons of the base ring. In Fig. 7, three inner-sphere water

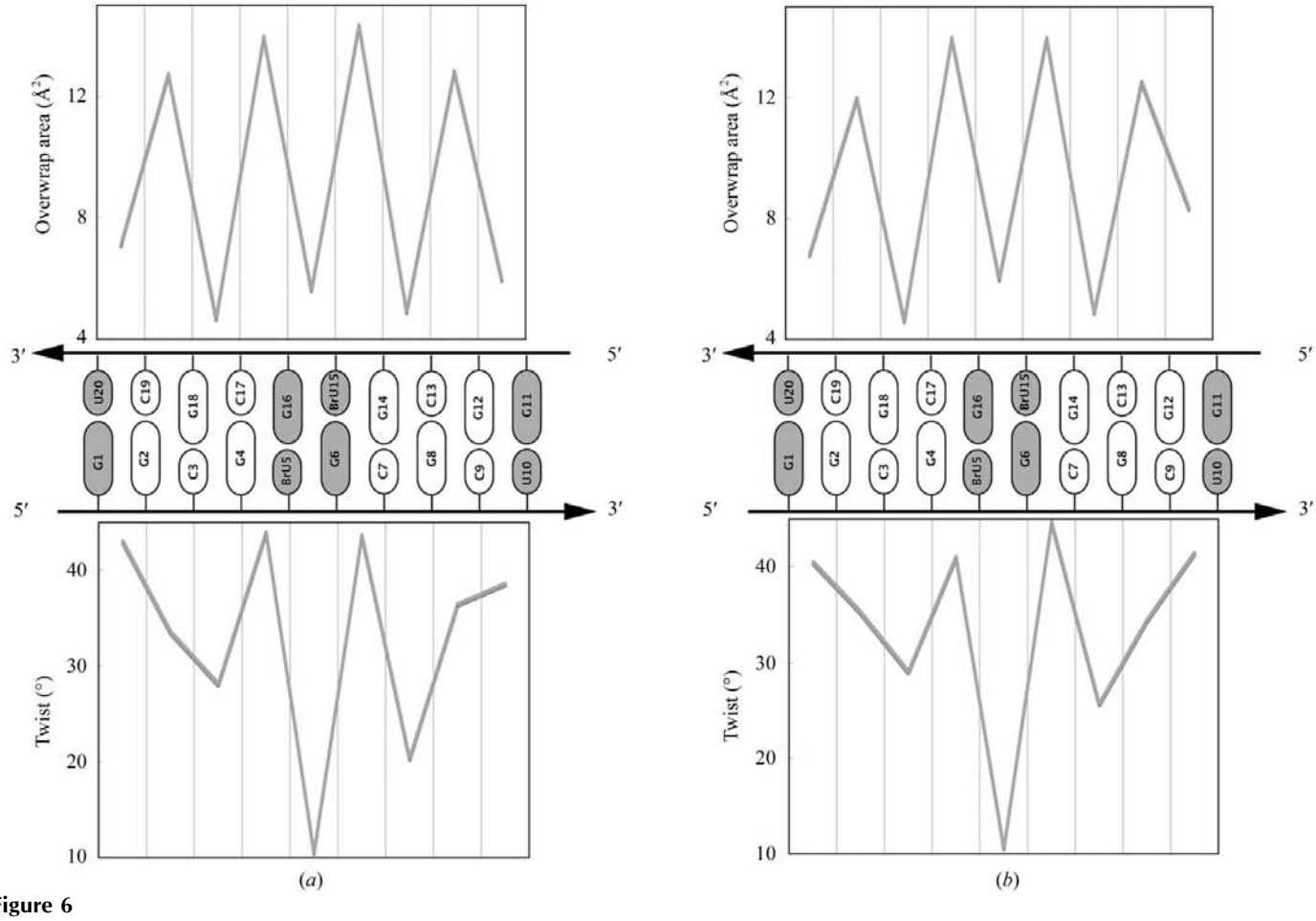

Figure 6
Base-overlap areas and twist angles at each base step in duplexes *A* (*a*) and *B* (*b*).

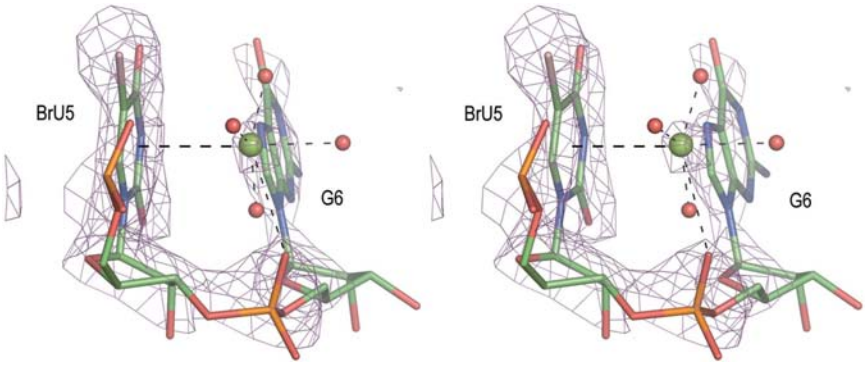

Figure 7
$2F_o - F_c$ map contoured at 2.5σ around the Mg^{2+}-binding site in duplex *A*. The yellow sphere is Mg^{2+} ion and the small red spheres are coordinated water molecules.

molecules and the phosphate O atom form a square parallel to the BrU5 ring. The ionic core appears to interact pervasively with the face of the base, as observed in Fig. 7. If the centroid of BrU5 corresponds to the axial position, the Mg^{2+} ion could complete an octahedral coordination sphere together with the fourth water molecule at another axial position.

3.5. Biological implications

The terminal G·U base pairs, which form a '5′-end G·U base pair' in the RNA duplex, have good base-pair stacking with the adjacent Watson–Crick G·C base pairs (Fig. 5*a* and 5*e*) and also base stacking of Gs by crystal packing as shown in Fig. 4(*a*). In contrast, our attempts to crystallize the same RNA duplex but with the terminal G·U base pairs switched to '5′-end U·G base pairs' were unsuccessful. This is probably because '5′-end U·G base pairs' have poor base stacking with the adjacent Watson–Crick base pairs. On the other hand, even for internal G·U base pairs, Us (BrU5 in the present structure) show unstacked bases at the 3′-side (Fig. 5*c*). It should be noted that the Mg^{2+} ion interacts with BrU5, one of the unstacked bases, through a cation–π interaction and may contribute to stabilization of unstacked bases. Thus, stacking must be the major factor that stabilizes the G·U base pairs. In this context, it is of interest that the specific cleavages in group I introns (Bevilacqua *et al.*, 1994) and HDV ribozymes (Perrotta & Been, 1996) and the photocleavages induced by organic or metal compounds (Burgstaller & Famulok, 1997; Burgstaller *et al.*, 1997; Chow & Barton, 1992; Hickerson *et al.*, 1998) occur at nucleotides adjacent to G·U pairs. All of these known G·U pairs induce strand scission on the 3′-side of U, which has been characterized as the 'poor stacking' or low-twist angle side of the G·U pair (Fig. 6). This cleavage leaves stable fragments ending with the '5′-end G·U pair', characterized as 'good stacking' with the adjacent base pair.

We thank Professor N. Sakabe for help during data collection at Photon Factory BL-6B. This research was supported in part by Special Coordination funds of ORCS for promoting Science and Technology (to HM) from the Ministry of Education, Science, Sports and Culture of Japan.

References

Adams, P. L., Stahley, M. R., Kosek, A. B., Wang, J. & Strobel, S. A. (2004). *Nature (London)*, **430**, 45–50.
Arai, S., Chatake, T., Ohhara, T., Kurihara, K., Tanaka, I., Suzuki, N., Fujimoto, Z., Mizuno, H. & Niimura, N. (2005). *Nucleic Acids Res.* **33**, 3017–3024.
Benard, L., Mathy, N., Grunberg-Manago, M., Ehresmann, B., Ehresmann, C. & Portier, C. (1998). *Proc. Natl Acad. Sci. USA*, **95**, 2564–2567.
Bevilacqua, P. C., Li, Y. & Turner, D. H. (1994). *Biochemistry*, **33**, 11340–11348.
Biswas, R. & Sundaralingam, M. (1997). *J. Mol. Biol.* **270**, 511–519.
Biswas, R., Wahl, M. C., Ban, C. & Sundaralingam, M. (1997). *J. Mol. Biol.* **267**, 1149–1156.
Brünger, A. T., Adams, P. D., Clore, G. M., DeLano, W. L., Gros, P., Grosse-Kunstleve, R. W., Jiang, J.-S., Kuszewski, J., Nilges, M., Pannu, N. S., Read, R. J., Rice, L. M., Simonson, T. & Warren, G. L. (1998). *Acta Cryst.* D**54**, 905–921.
Burgstaller, P. & Famulok, M. (1997). *J. Am. Chem. Soc.* **119**, 1137–1138.
Burgstaller, P., Hermann, T., Huber, C., Westhof, E. & Famulok, M. (1997). *Nucleic Acids Res.* **25**, 4018–4027.
Chow, C. S. & Barton, J. K. (1992). *Biochemistry*, **31**, 5423–5429.
Crick, F. H. C. (1966). *J. Mol. Biol.* **19**, 548–555.
Deng, J. & Sundaralingam, M. (2000). *Nucleic Acids Res.* **28**, 4376–4381.
Egli, M., Portmann, S. & Usman, N. (1996). *Biochemistry*, **35**, 8489–8494.
Ennifar, E., Walter, P. & Dumas, P. (2003). *Nucleic Acids Res.* **31**, 2671–2682.
Gautheret, D., Konings, D. & Gutell, R. R. (1995). *RNA*, **1**, 807–814.
Gutell, R. R., Larsen, N. & Woese, C. R. (1994). *Microbiol. Rev.* **58**, 10–26.
He, L., Kierzek, R., SantaLucia, J. Jr, Walter, A. E. & Turner, D. H. (1991). *Biochemistry*, **30**, 11124–11132.
Hickerson, R. P., Watkins-Sims, C. D., Burrows, C. J., Atkins, J. F., Gesteland, R. F. & Felden, B. (1998). *J. Mol. Biol.* **279**, 577–587.
Holbrook, S. R., Cheong, C., Tinoco, I. Jr & Kim, S.-H. (1991). *Nature (London)*, **353**, 579–581.
Leonard, G. A., McAuley-Hecht, K. E., Ebel, S., Lough, D. M., Brown, T. & Hunter, W. N. (1994). *Structure*, **2**, 483–494.
McFail-Isom, L., Shui, X. & Williams, L. D. (1998). *Biochemistry*, **37**, 17105–17111.
McRee, D. E. (1999). *J. Struct. Biol.* **125**, 156–165.
Masquida, B., Sauter, C. & Westhof, E. (1999). *RNA*, **5**, 1384–1395.
Masquida, B. & Westhof, E. (2000). *RNA*, **6**, 9–15.
Misra, V. K. & Draper, D. E. (1998). *Biopolymers*, **48**, 113–135.
Mizuno, H. & Sundaralingam, M. (1978). *Nucleic Acids Res.* **5**, 4451–4461.
Niimura, N., Arai, S., Kurihara, K., Chatake, T., Tanaka, I. & Bau, R. (2005). *Hydrogen- and Hydration-Sensitive Structural Biology*, edited by N. Niimura, H. Mizuno, J. R. Helliwell & E. Westhof, pp. 17–35. Tokyo: KubaPro.
Nikulin, A., Serganov, A., Ennifar, E., Tishchenko, S., Nevskaya, N., Shepard, W., Portier, C., Garber, M., Ehresmann, B., Ehresmann, C., Nikonov, S. & Dumas, P. (2000). *Nature Struct. Biol.* **7**, 273–277.
Ogle, J. M., Brodersen, D. E., Clemons, W. M. Jr, Tarry, M. J., Carter, A. P. & Ramakrishnan, V. (2001). *Science*, **292**, 897–902.Olson, W. K., Bansal, M., Burley, S. K., Dickerson, R. E., Gerstein, M.,

Harvey, S. C., Heinemann, U., Lu, X. J., Neidle, S., Shakked, Z., Sklenar, H., Suzuki, M., Tung, C. S., Westhof, E., Wolberger, C. & Berman, H. M. (2001). *J. Mol. Biol.* **313**, 229–237.
Otwinowski, Z. & Minor, W. (1997). *Methods Enzymol.* **276**, 307–326.
Pan, Y., Priyakumar, U. D. & MacKerell, A. D. Jr (2005). *Biochemistry*, **44**, 1433–1443.
Park, S. J., Hou, Y. M. & Schimmel, P. (1989). *Biochemistry*, **28**, 2740–2746.
Perrotta, A. T. & Been, M. D. (1996). *Nucleic Acids Res.* **24**, 1314–1321.
Robinson, H., Gao, Y. G., Sanishvili, R., Joachimiak, A. & Wang, A. H. (2000). *Nucleic Acids Res.* **28**, 1760–1766.
Serra, M. J., Baird, J. D., Dale, T., Fey, B. L., Retatagos, K. & Westhof, E. (2002). *RNA*, **8**, 307–323.
Simpson, L. & Thiemann, O. H. (1995). *Cell*, **81**, 837–840.
Stout, C. D., Mizuno, H., Rubin, J., Brennan, T., Rao, S. T. & Sundaralingam, M. (1976). *Nucleic Acids Res.* **3**, 1111–1123.
Strobel, S. A. & Cech, T. R. (1995). *Science*, **267**, 675–679.
Szymanski, M., Barciszewska, M. Z., Erdmann, V. A. & Barciszewski, J. (2000). *Mol. Biol. Evol.* **17**, 1194–1198.
Trikha, J., Filman, D. J. & Hogle, J. M. (1999). *Nucleic Acids Res.* **27**, 1728–1739.
Westhof, E., Dumas, P. & Moras, D. (1988). *Biochimie*, **70**, 145–165.
Wu, M., McDowell, J. A. & Turner, D. H. (1995). *Biochemistry*, **34**, 3204–3211.
Zaric, S. D., Popovic, D. M. & Knapp, E. W. (2000). *Chem. Eur. J.* **6**, 3935–3942.